Oxidation resistance of Zr- and Hf-diboride composites containing SiC in air plasma up to 2600 K for aerospace applications

C. Pellegrini, M. Balat-Pichelin, O. Rapaud, E. Bêche

Ceramics International 48 (2022) 2177–2190

Contents lists available at ScienceDirect

Ceramics International

journal homepage: www.elsevier.com/locate/ceramint

Oxidation resistance of Zr- and Hf-diboride composites containing SiC in air plasma up to 2600 K for aerospace applications

C. Pellegrini [a,b], M. Balat-Pichelin [a,*], O. Rapaud [b], E. Bêche [a]

[a] PROMES-CNRS, UPR8521, 7 Rue Du Four Solaire, 66120, Font-Romeu Odeillo, France
[b] IRCER-CNRS, UMR 7315, Centre Européen de La Céramique, 12 Rue Atlantis, 87068, Limoges, France

ARTICLE INFO

Keywords:
UHTC
SiC
Oxidation
Air plasma
High temperature

ABSTRACT

Microstructure-controlled and fully-dense ZrB_2 and HfB_2 composites were elaborated by Spark Plasma Sintering with two different amounts of SiC (20 and 30 vol%) added to improve their oxidation resistance using optimized sintering parameters. Oxidation of several samples in air plasma conditions, at 1000 Pa total pressure and from 1800 K up to 2600 K, was carried out. The mass variation of samples during oxidation duration of 300 s on a temperature plateau was followed. A four-step oxidation mechanism, identified by four singular mass variation behaviors depending on the oxidation temperature ranges, was proposed and detailed. The total normal emissivity was measured on pre-oxidized samples and high values around 0.90 were obtained from 1300 to 1900 K due to the presence of the oxide layer formed in air plasma conditions and this high emissivity is interesting for aerospace applications.

1. Introduction

Ultra-high temperature ceramics (UHTCs) are promising for extreme environments, including very high temperatures (more than 2000 K) and oxidizing atmosphere [1,2]. UHTCs are mainly composed of carbides, nitrides, borides and silicides with very high melting points (higher than 3000 K) [3]. Among these different classes, borides, specifically ZrB_2 and HfB_2 are considered as the most promising candidates for aerospace applications due to their oxidation into refractory oxides. However, a volatilization of the boron oxide appears since 1373 K and let the protective oxide layer porous, according to the following reactions:

$$ZrB_2\ (s) + O_2\ (g) \rightarrow ZrO_2\ (s) + B_2O_3\ (g) \quad (1)$$

$$HfB_2\ (s) + O_2\ (g) \rightarrow HfO_2\ (s) + B_2O_3\ (g) \quad (2)$$

Additional compounds have been considered to improve the oxidation resistance of the diborides. The most common one is silicon carbide and earlier studies on oxidation resistance of boride-SiC systems have begun in the late 60's and 70's up to 1773 K [4,5]. Diboride-based composites with silicon carbide as additional compound have been largely studied with different sintering methods (Hot Pressing or Spark Plasma Sintering, simplified by HP or SPS respectively) and in different conditions sometimes away from the application conditions. Earth atmospheric re-entry conditions include low oxygen partial pressure, atomic oxygen, and temperatures higher than 2000 K. The typical amounts encountered in association with ZrB_2 are 20 vol% and 30 vol% of SiC and few studies concern HfB_2. In the following sections, the literature relative to the oxidation of these composites has been summarized according to the different atmospheres: ambient air, flowing or static, and dissociated air with the presence of atomic oxygen. Moreover, oxidation using oxyacetylene torches with a more complex and different gas composition is also reported.

1.1. Oxidation in ambient air conditions (molecular oxygen)

Studies carried out in ambient air conditions are briefly detailed in this section, firstly at atmospheric pressure, followed by low-pressure experiments. Williams et al. have studied the isothermal oxidation of ZrB_2 composites with several SiC amounts, from 20 vol% to 80 vol%, sintered by HP, under static air in a furnace at 1773 K for 50 h at atmospheric pressure [6]. The increasing of SiC amount seems to be beneficial due to the formation of a silica protective layer with some isolated ZrO_2 grains. The composites with more than 65% SiC have presented undetectable SiC-depleted layer unlike other compositions containing lower amounts of SiC. Inoue et al. have studied the oxidation

* Corresponding author.
E-mail address: Marianne.balat@promes.cnrs.fr (M. Balat-Pichelin).

https://doi.org/10.1016/j.ceramint.2021.09.310
Received 29 June 2021; Received in revised form 9 September 2021; Accepted 30 September 2021
Available online 4 October 2021

Table 1
Composition and imposed temperature during the SPS cycle.

Sample name	Z70S30	Z80S20	H70S30	H80S20
Diboride (ZrB_2 or HfB_2) content (vol %)	70	80	70	80
SiC content (vol%)	30	20	30	20
Imposed temperature (K)	1823	1923	1923	2023

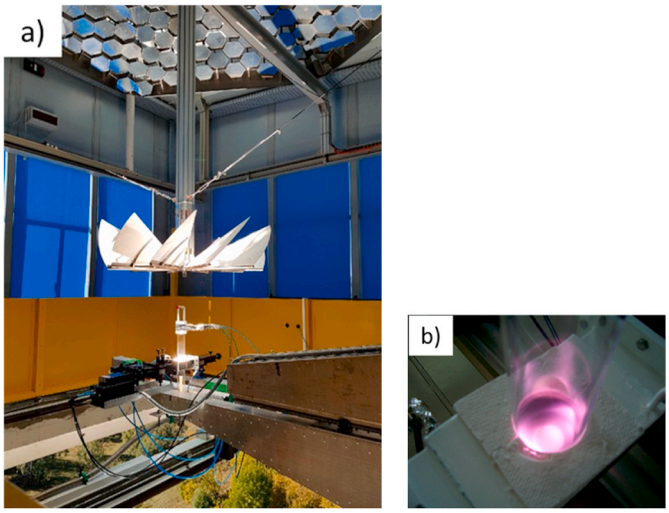

Fig. 1. a) MESOX facility at the focus of the 6 kW Odeillo solar furnace and b) image of the air plasma with a sample inside.

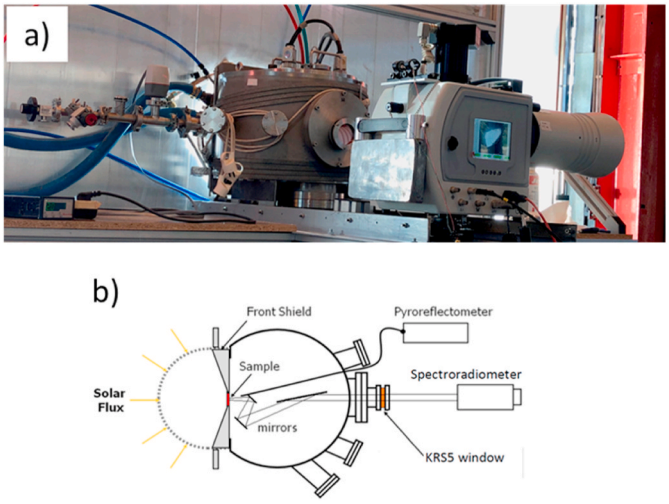

Fig. 2. a) Picture and b) scheme of the set-up MEDIASE implemented at the focus of the 1 MW solar furnace.

behavior at 2273 K of ZrB_2 with different amounts of SiC (0–30 vol%) sintered by SPS under air atmosphere using an electric heating system during 10 s [7]. The porosity of the SiC-depleted layer increased as the SiC content in the ZrB_2–SiC composites increased due to the greater quantity of consumed SiC. A too high amount of SiC (30 vol% in Inoue's study) seems detrimental against oxidation up to 2000 K as also observed by Williams et al. at a lower temperature [6]. Han et al. have also studied the oxidation of ZrB_2 composites with 10, 20 and 30 vol% at 2173 K in air during 1 h and the best oxidation resistance composition was with 20 vol%. For this composite, the oxide layer was dense and adherent [8]. Carney sintered HfB_2-20 vol%SiC samples by SPS and oxidized them from 1673 to 2273 K in a furnace in ambient atmosphere

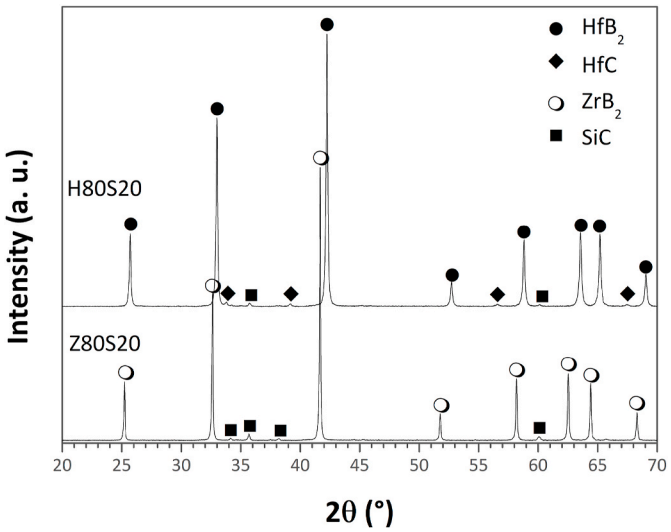

Fig. 3. XRD patterns of H80S20 and Z80S20 after sintering.

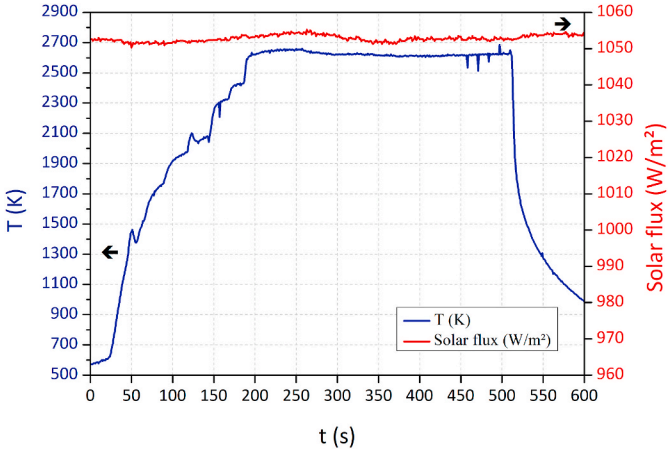

Fig. 4. Example of a temperature profile versus time together with the incident solar flux.

during 1 h holding time [9]. Up to 2273 K, the critical factors that influence the oxidation resistance is the flow of SiO_2 glass and the emergence of porosities in the HfO_2 oxide layer. Piriou et al. have studied HfB_2-based composites sintered by SPS containing various amounts of SiC (0 up to 30 vol%). The results of oxidation in air at 1800 K with a thermogravimetric analysis (TGA) have highlighted that HfB_2-20 vol% SiC was the most resistant with no mass change after 7 min exposure [10].

On the other hand, few authors have studied the effect of low oxygen partial pressures, in air, on the oxidation behavior at high temperature [11–14]. Li et al. have shown for ZrB_2-20 vol%SiC composites, sintered by HP, the effect of the oxygen partial pressure (from 60 000–10 Pa) on their oxidation behavior at 1773 K for 30 min [11]. They concluded that the thickness of the oxidized layer increased with the decreasing of the oxygen partial pressure down to 1000 Pa and for the two lowest pressures, the thickness decreases. Two combined phenomena can explain this observation: the volatilization of silica accelerated by the low total pressure and the active oxidation of SiC because of the high temperature and the low oxygen partial pressure. Seong et al. have sintered by HP ZrB_2-x vol%SiC (x = 0 to 40) and oxidized them at 1773 K in a furnace with a gas flow under $2x10^4$ Pa or 10^{-8} Pa of oxygen partial pressure [12]. As a result, the oxidation resistance of the composites is highly dependent on both the SiC amount and the oxygen partial pressure. The

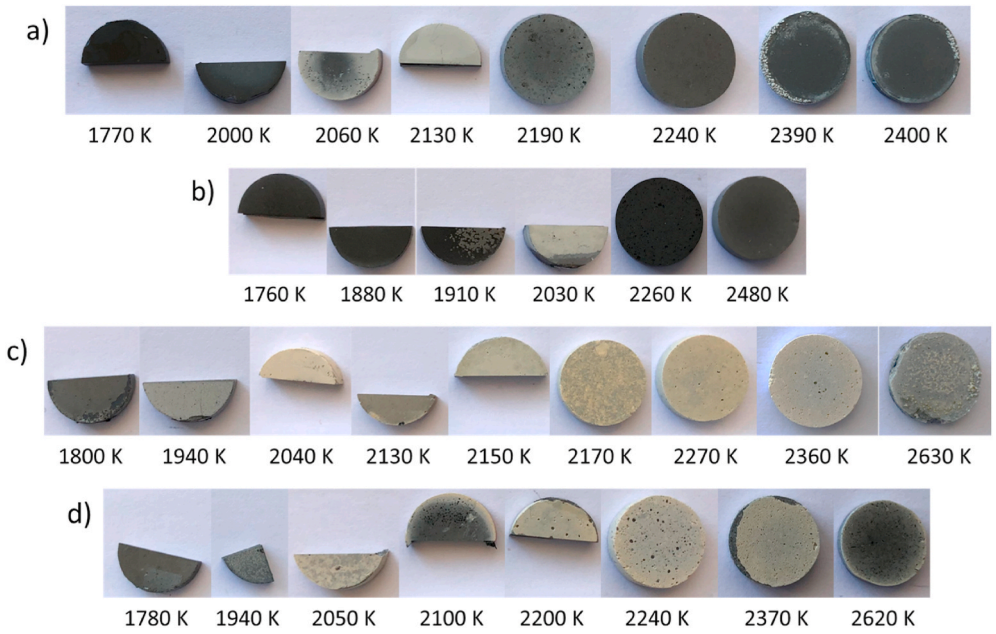

Fig. 5. Photos of the samples after oxidation in air plasma during 300 s for several temperatures for a) H80S20, b) H70S30, c) Z80S20 and d) Z70S30.

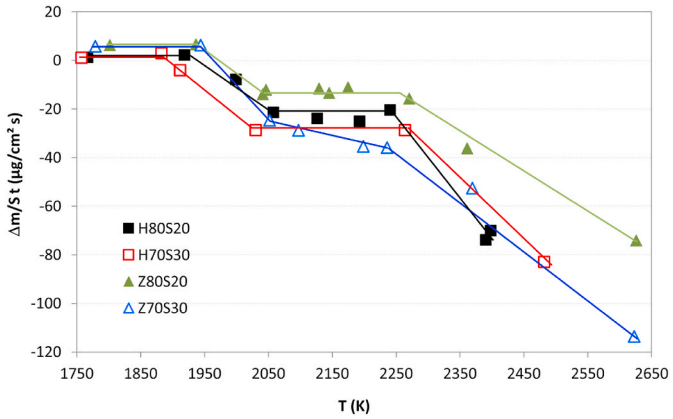

Fig. 6. Mass variation per unit area and time versus temperature for the four compositions.

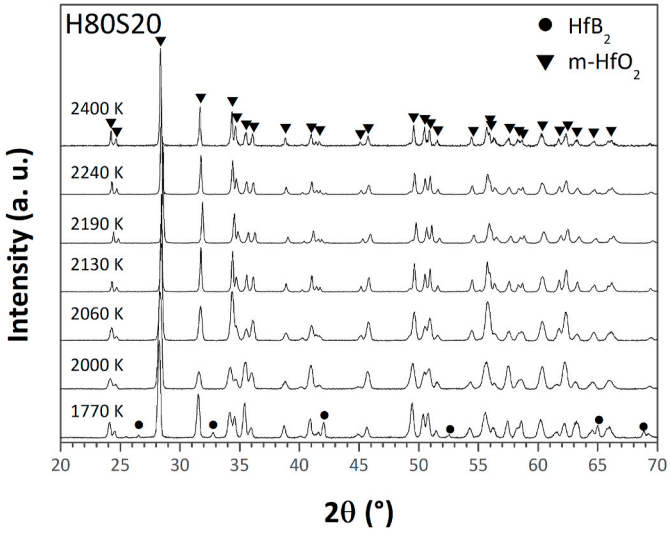

Fig. 7. XRD patterns for several H80S20 oxidized samples from 1770 to 2400 K.

ZrB_2-40 vol%SiC composite exhibited the lowest oxidation rate under $2x10^4$ Pa. Tian et al. have studied the oxidation of ZrB_2-20 vol%SiC sintered by HP from 500 to 1500 Pa oxygen partial pressure at 1773 K in a tubular furnace during 30 min [13]. They have shown that the oxidation resistance increased with the reduction of the oxygen partial pressure from 1500 down to 500 Pa. Yang et al. have sintered by HP ZrB_2-20 vol%SiC composite [14]. Oxidation testing were carried out using an induction heating ultra-high temperature oxidation testing apparatus reaching up to 2073 K at different pressures for 30 min. The ZrB_2-20 vol%SiC composite exhibited catastrophic oxidation behavior at 100 Pa oxygen partial pressure, with the formation of a thick non-protective porous ZrO_2 layer.

Thus, the impact of the oxygen partial pressure is clear as when the SiO_2 layer is volatilized – depending on the temperature conditions – only ZrO_2 crystals are remaining on the surface and the oxidation could be catastrophic.

1.2. Oxidation in dissociated air conditions (atomic oxygen)

Air plasma conditions have been considered in previous oxidation studies and the atomic oxygen can be generated by microwaves, arc-jet, plasma wind tunnel or plasmatron facilities [11,15–23]. Li et al. concluded that atomic oxygen – generated by microwaves – is very reactive and oxidizes the ZrB_2-20 vol%SiC composite faster than molecular oxygen at 1773 K with an increase of the thickness of the oxide layer by 1.5 times [11]. Du et al. introduced a ZrB_2-30 vol%SiC sample sintered by HP in a side-arm reactor (low enthalpy facility) at 1873 K in an atomic oxygen environment at 100 Pa total pressure [15]. The surface temperature increased to nearly 2163 K. The introduction of the sample in dissociated oxygen atmosphere leads to a violent oxidation of the composite associated to a high oxidation rate during the first seconds of the experiment. They concluded that this response was related to the competition between oxidation and catalytic reactions. Recently, Mungiguerra et al. have explored the effects of SiC amount associated to Y_2O_3 on the aero-thermal resistance of ZrB_2-based materials sintered by HP using arc-heated plasma wind tunnel in supersonic flow conditions [16]. ZrB_2 with 20 vol% of additional compound (18.5 vol%SiC- 5 vol% Y_2O_3) revealed the best behavior under aero-heating conditions up to 20

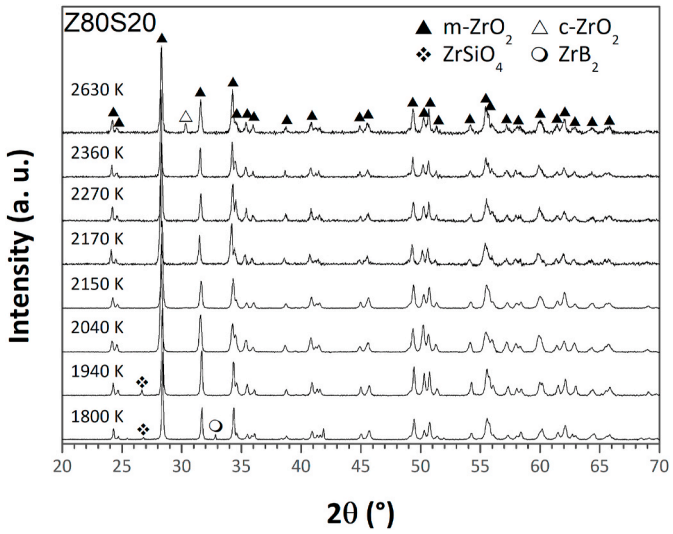

Fig. 8. XRD patterns for several Z80S20 oxidized samples from 1800 to 2630 K.

MJ/kg specific total enthalpy with only a thickness of 150 μm for the oxide scale that was compact and smooth. Gasch and Johnson have oxidized dense HfB_2-20 vol%SiC samples elaborated by HP or by SPS for comparison in the NASA Ames arc-jet facility during 10 min at respectively 1963 K and 1803 K and they have observed that the SiC depletion was higher for the HP sample (24 μm) compared to the SPS one (8 μm) with respective thicknesses of the oxide layer of 13 and 3 μm [17]. The reduced grain size of the SPS sample was responsible of the better oxidation resistance. The oxidation of HfB_2-based composites containing 20 vol% SiC sintered by HP has been studied by Poerschke et al. in air at 7000 Pa at 2630 K during 10 min using the same NASA Ames arc-jet facility [18]. After testing, the samples presented an oxide layer composed of a first layer of 390 μm of porous HfO_2 and a second SiC-depleted layer of 740 μm above the undamaged HfB_2. Using the 1.2 MW plasmatron of VKI (Von Karman Institute, Belgium), Marschall et al. have studied the oxidation of ZrB_2-30 vol% SiC composite, sintered by HP, during 20 min up to 1850 K [19]. The sample was covered by a glassy layer with some ZrO_2 isolated grains. The thickness of the oxide layer decreased when the temperature increased for 10 min oxidation. They also confirmed that the oxidation is faster in dissociated air. Hu et al. oxidized ZrB_2–SiC (10–30 vol%) elaborated by HP and they demonstrated that the 30 vol% composition was the best one for its oxidation resistance at 2273 K under 18 000 Pa [20]. Sevastyanov et al. sintered porous HfB_2-based composites containing from 10 up to 45 vol % SiC by SPS (around 35% porosity after sintering) [21–23]. These composites were oxidized in a high-enthalpy dissociated air stream using the 100 kW induction plasmatron of IPM (Institute for Problems in Mechanics, Moscow, Russia) at total pressures going from 100 to 200 hPa and up to 3000 K during 40 min maximum. The mass variation of the samples was different according to the sample composition with a mass loss measured for the 15 and 20 vol% SiC compositions and a mass gain for the 10 vol% one. The porous surfaces were mainly composed of big crystals of monoclinic HfO_2 with sometimes traces of $HfSiO_4$ due to the melting with the residual borosilicate glass.

1.3. Oxidation with torches

Oxyacetylene and other torches yield flames with very complex gas composition not always clearly characterized. They are not fully representative of an atmospheric entry or high-speed conditions. Nevertheless, it is a common and useful facility to perform preliminary characterization of UHTC materials. Williams et al. have studied the oxidation of ZrB_2–SiC (20–80 vol%) composites under CH_4–O_2 torch at 2073 K for 20 min [6]. They concluded that ZrB_2-based composites with the greatest amounts of SiC (80 and 65 vol%) exhibit a depression on the hotter zone of the surface attributed to the vaporization of silica. Han et al. have concluded that the ZrB_2-20 vol% SiC composite presents an excellent oxidation resistance under oxyacetylene torch at 2473 K with an oxidized layer of 375 μm after 10 min oxidation [24]. Carney et al. have studied the oxidation behavior of HfB_2-20 vol% SiC composite, sintered by SPS, under an oxyacetylene torch at 2473 K for 200 s [25]. They concluded that the oxide scale is composed of multiple layers that were non-adherent to the undamaged material.

1.4. Summary and aim of our study

ZrB_2-based composites containing SiC have been largely studied compared to HfB_2 ones. Among the most common amount of SiC with these diborides, 20 vol% and 30 vol% are the most frequently studied compositions. The most used sintering methods for these materials are firstly HP and secondly SPS. The conclusion of most of the studies presented above is that the diboride HfB_2 or ZrB_2 associated with SiC seems promising for applications under dissociated air and very high temperatures. For most of the studies, depending on the pressure and temperature conditions, the oxide layer formed on these UHTC consists of a first layer composed of SiO_2 or borosilicate glass with ZrO_2 or HfO_2 isolated grains, a second layer made of pure zirconia or hafnia and finally a third SiC-depleted layer above the undamaged ZrB_2–SiC or HfB_2-SiC composites.

Our study brings a new light on these systems by combining fully-dense composites sintered by SPS – with optimized parameters to

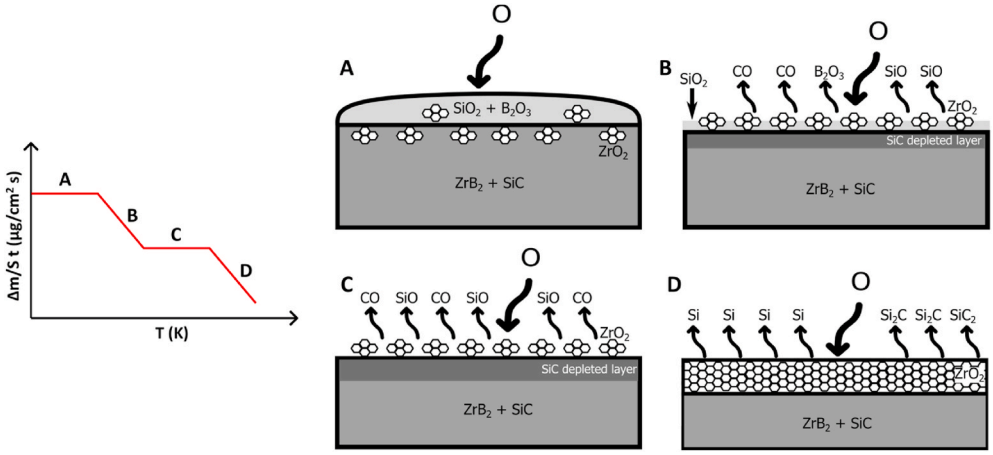

Fig. 9. Scheme of the different oxidation mechanisms.

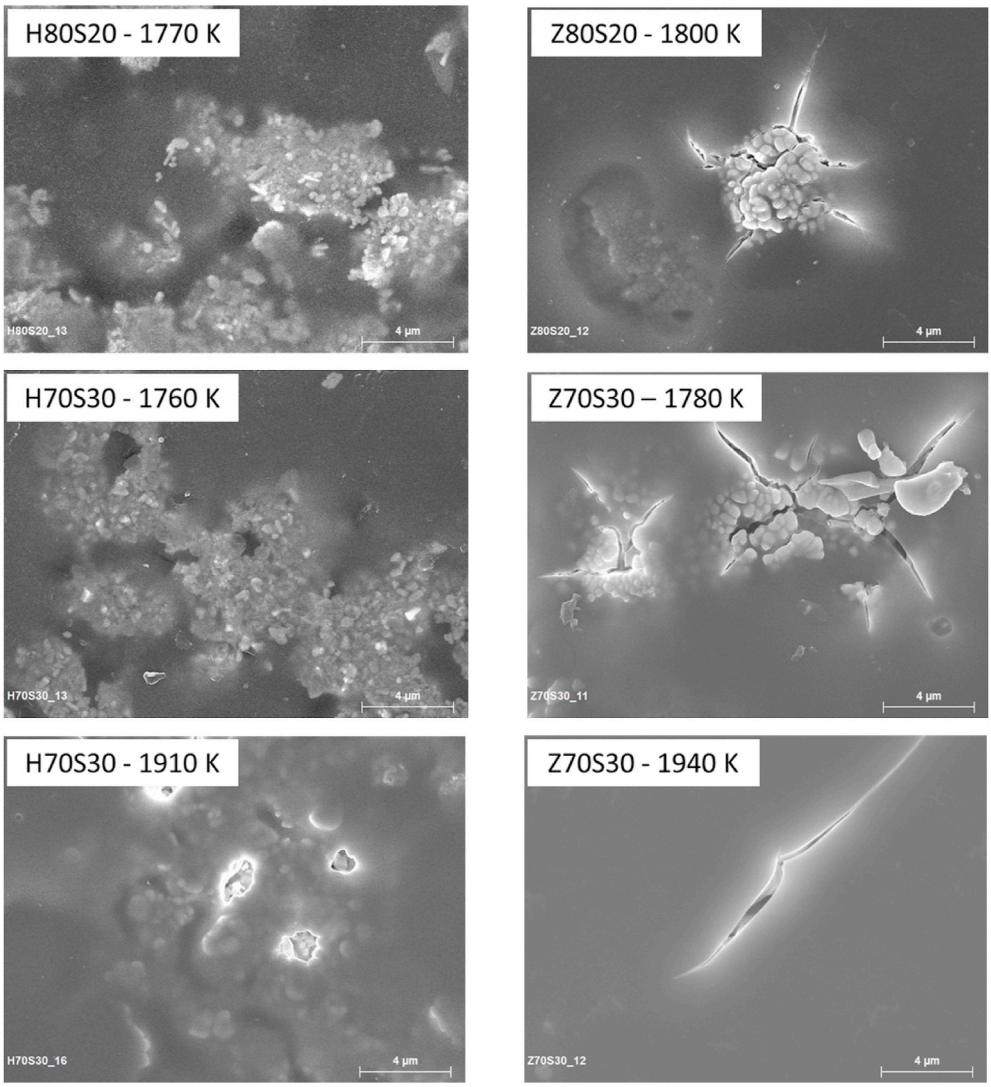

Fig. 10. SEM images of the oxidized surfaces from segment A (x 6000, scale bar 4 µm).

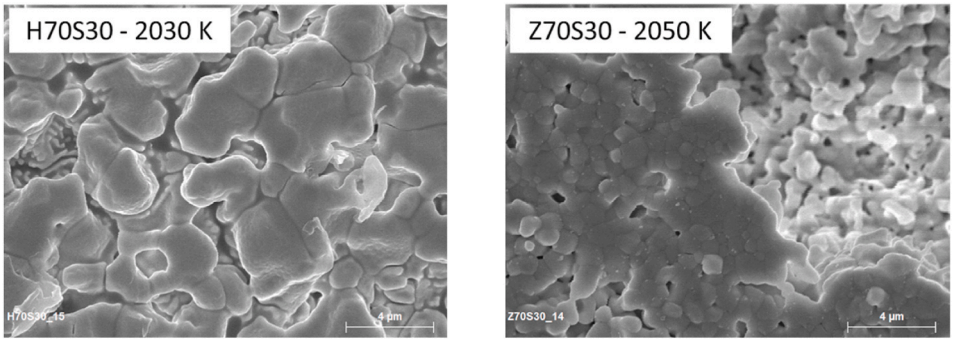

Fig. 11. SEM images of the oxidized surfaces from segment B (x 6000, scale bar 4 µm).

avoid the detrimental effect of porosity on oxidation resistance –, low total pressure, atomic oxygen, temperature greater than 2000 K which is partly different from the existing literature. The aim of this work is to study the oxidation mechanisms occurring at very high temperatures, up to 2600 K, in air plasma conditions for diboride-based composites containing 20 vol% or 30 vol% of SiC with a controlled and dense microstructure obtained by SPS. Moreover, the measurement of the total emissivity was performed as it is an important parameter for aerospace applications, as the hot parts of the vehicle can be submitted to very high temperatures during a hypersonic entry and the materials must have the highest emissivity to reject the heat. This is why we have measured and presented the values obtained on samples pre-oxidized in air plasma conditions that are more representative of the surface state of the heat shield materials of the space vehicle.

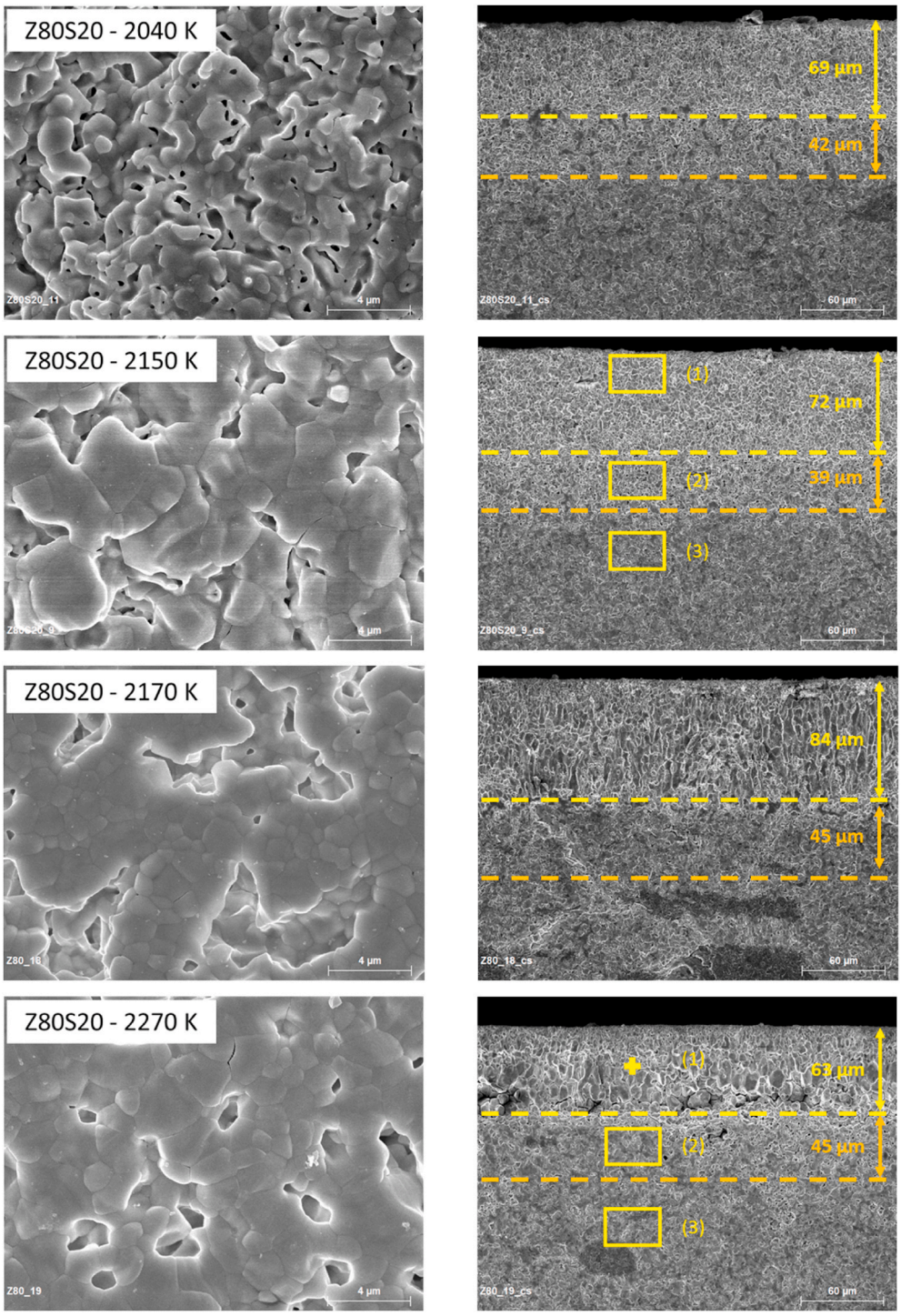

Fig. 12. SEM images of the oxidized surfaces and corresponding cross-sections for the samples on the plateau C for the Z80S20 composite (scale bars: 4 µm for the surfaces and 60 µm for the cross-sections).

2. Materials and methods

In this section, the sample elaboration, the oxidation method, the method used for emissivity measurements and the material characterization techniques are presented.

2.1. Sample elaboration

Commercial powders, HfB_2 powder (99.5% purity, $d_{50} = 22$ µm, $\rho = 11$ g cm^{-3}, from abcr, Germany), ZrB_2 powder (97% purity, $d_{50} = 5.7$ µm, $\rho = 6$ g cm^{-3}, from H.C. Starck, Germany) and SiC powder (α-SiC, > 98.5% purity, $d_{50} = 1$ µm, $\rho = 3.2$ g cm^{-3}, from H.C. Starck, Germany) were chosen as raw materials. HfB_2 powder was grinded at a $d_{50} = 5.4$ µm before sintering to control the microstructure and to obtain equivalent grain size for each composite.

First, the grain size of HfB_2 powder has been refined by planetary milling with the following protocol: 5 cycles of 6 min split into 1 min milling followed by 5 min break to prevent heating. ZrB_2 powder already has the required size. WC balls were used in a WC media. HfB_2 refined powder or ZrB_2 powder were mixed with SiC powder for one cycle

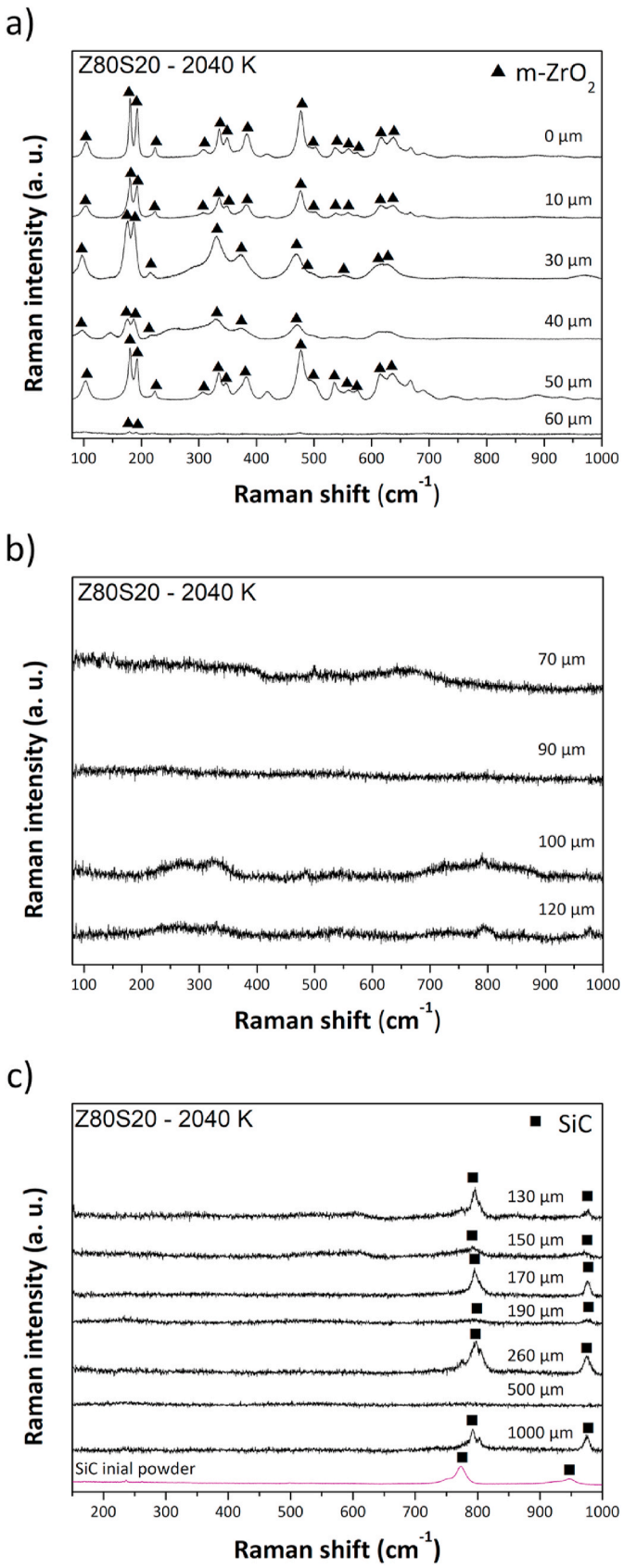

Fig. 13. Raman spectra obtained on the cross-section at different positions from the surface (0 µm) down to 1000 µm in depth for the Z80S20 sample oxidized at 2040 K.

described above to homogenize the powder. Milled powders have been characterized by X-Ray fluorescence to investigate the presence of eventual WC contamination during milling and no impurities were found.

Mixtures were introduced in a graphite die (inner diameter 13 mm for oxidation study and 25 mm for emissivity measurements), pre-compacted at 75 MPa, lined with a graphitized paper (Papyex, Mersen, France) and sintered using Spark Plasma Sintering (Dr Sinter 825, Fuji Electronics Industrial Co. Ltd., Japan). The temperature was monitored by an optical pyrometer at the external surface of the die. Sintering parameters were optimized by decreasing the imposed temperatures according to the SiC amount (Table 1). Fully dense samples were obtained with optimized conditions (holding time and temperature, applied pressure). The sintering protocols are based on the one developed by Piriou et al. [10]. Every sintering cycle was carried out in vacuum, using a heating rate of 100 K/min with an applied load of 100 MPa and 10 min holding time. To simplify the names of the composites, H or Z and S letters, attributed to the HfB_2 or ZrB_2 and SiC phases respectively, are followed by the volume percent of HfB_2 or ZrB_2 and SiC constituting the composite.

The bulk density was measured using the method based on Archimede principle with ethanol as immersing medium. The relative density of each sintered material was evaluated by the ratio between the measured density and the theoretical density of powders calculated from the initial compositions using the rule of mixture.

2.2. Oxidation

The high temperature oxidation of the samples was carried out using the MESOX ('Moyen d'Essai Solaire d'OXydation' in French, Solar set-up for oxidation) reactor placed at the focus of the 6 kW Odeillo solar furnace. The device is represented in Fig. 1 with an image of the air plasma surrounding a sample and already detailed in [26].

The experimental parameters were chosen to partially reproduce the atmospheric re-entry conditions on Earth. The total air pressure was fixed at 1000 Pa, representing a pressure encountered during the re-entry phase in between 80 and 60 km altitude where the dissociation of atomic oxygen occurs due to the speed of the vehicle. A microwave air plasma is generated around the sample (300 W) containing about 70–80% atomic oxygen [27]. The sample is placed in the quartz tube, the plasma is ignited then the shutter is opened and the temperature rise of the sample lasts only a few tens of seconds to reach a plateau at the targeted temperature, maintained during 300 s. The sample is then rapidly cooled down by closing the shutter and stopping the plasma. The study was conducted over a temperature range from 1800 to 2600 K. The samples are weighed before and after oxidation using a precise balance (Ohaus Adventurer AX224, 0,1 mg accuracy).

2.3. Method for the emissivity measurements

Emissivity measurements in air conditions at low pressure (1000 Pa) on pre-oxidized samples in the above air plasma conditions have been made using the experimental set-up MEDIASE implemented at the focus of the 1 MW solar furnace (Fig. 2). The direct method used at PROMES-CNRS laboratory is the one that corresponds directly to the definition of the emissivity: the directional spectral radiance (L'_λ) of the material is measured as well as its temperature to calculate the spectral radiance of the blackbody (L^0_λ) at the same temperature [28]. The ratio of the radiances gives the spectral directional emissivity:

$$\varepsilon'_\lambda = L'_\lambda / L^0_\lambda$$

In this study due to the size of the samples, 25 mm diameter, only the normal spectral emissivity was measured and the normal total emissivity was calculated.

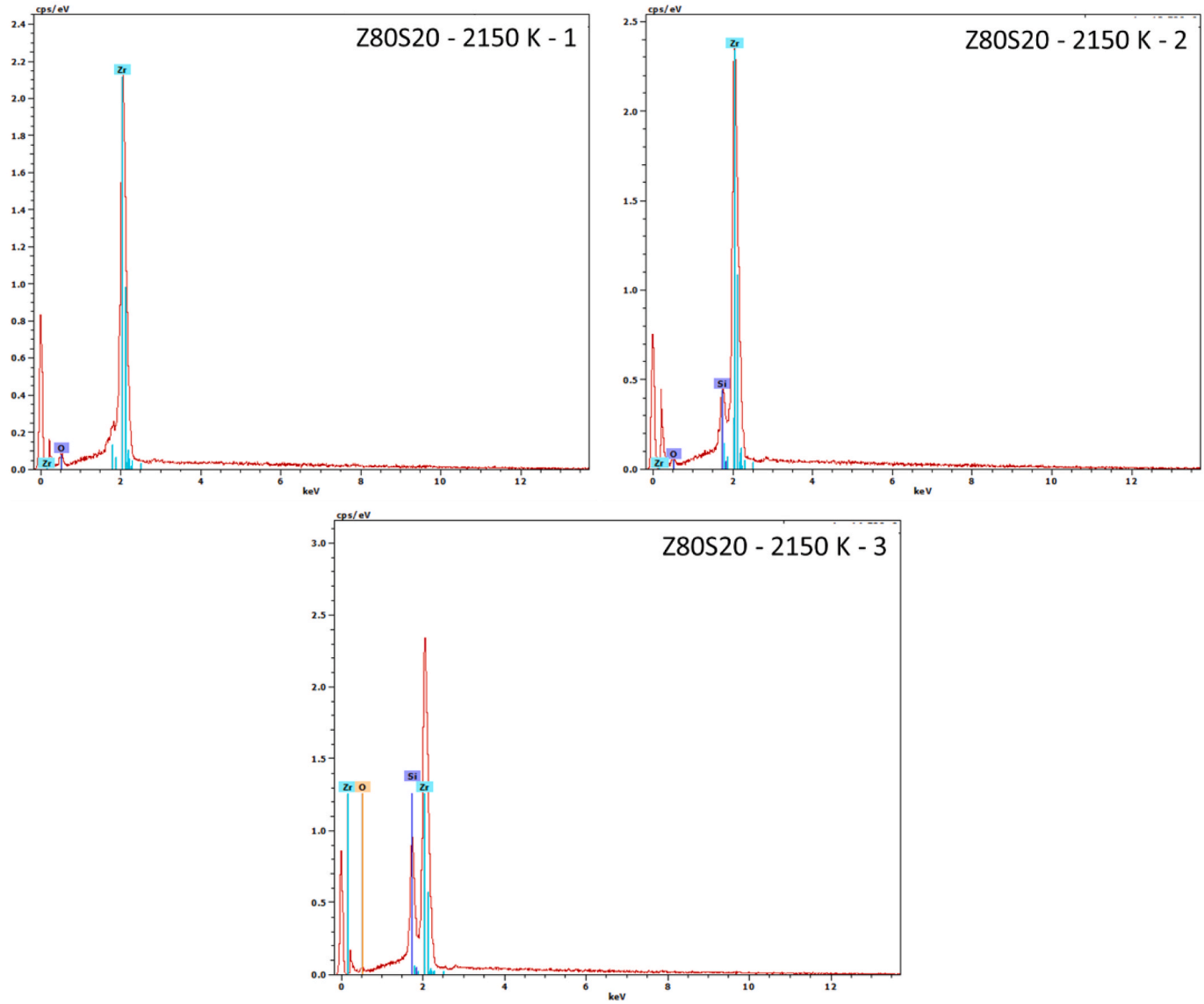

Fig. 14. EDS spectra obtained on the cross-section of the Z80S20 sample oxidized at 2150 K (analysis zones 1, 2 and 3 marked in Fig. 12).

2.4. Materials characterization

Scanning electron microscopy (SEM) and Energy Dispersive Spectroscopy (EDS) analyses were done using a Hitachi S-4500 SEM-FEG microscope. X-ray diffraction (XRD) analyses were performed using a PANalytical XPert Pro diffractometer (Cu Kα radiation, $\lambda = 1.5418$ Å). X-ray diffraction measurements of θ-θ symmetrical scans were made over an angular range of 20–70°. The step size and the time per step were fixed at 0.017° and 10 s, respectively. The X-ray diffractograms were recorded and studied using PANalytical softwares (Data collector and HighScorePlus). Raman measurements were performed using a micro-Raman spectrometer (LabRAM HR Evolution, HORIBA Scientific, France). Raman spectra were collected along the cross-section of the oxidized samples every 10 μm from 0 to 100 μm. A 633 nm laser was used for ZrB_2–SiC samples due to the luminescence phenomenon caused by zirconia formation on the surface. In the non-oxidized layer, composed of diboride and SiC, the Raman spectra were obtained only for the SiC phase since the ZrB_2 or HfB_2 phases are Raman inactive.

3. Experimental results and discussion

In this section, the characterization of the sintered samples and the experimental results obtained for the oxidation are presented followed by a proposal for the explanation of the oxidation mechanisms. The experimental results obtained for the normal emissivity are also given.

3.1. Characterization of the sintered samples

After sintering by SPS, the samples were characterized by SEM to make sure that the samples present a good and homogeneous distribution of the SiC and diboride grains [10]. The average size of the diboride grains is around 5 μm and 1 μm for the SiC ones. Moreover, no porosity can be seen on the surface and this was confirmed by the density measurements. In this study, the grain size and the relative density have been set carefully because they can affect the oxidation resistance as previously observed by Gasch and Johnson [17].

The XRD diffractograms shown in Fig. 3 present the primary phases: the diboride, HfB_2 (ICDD 038–1398) or ZrB_2 (ICDD 034–0423) and the α-SiC (ICDD 075–8314). However, a secondary phase which can be considered as negligible has been detected only for the hafnium-based composite, HfC (ICDD 039–1491), due to the impurities present in the initial HfB_2 powder. The XRD patterns presented in Fig. 3 are for H80S20 and Z80S20, but similar results were obtained for both the H70S30 and Z70S30 compositions.

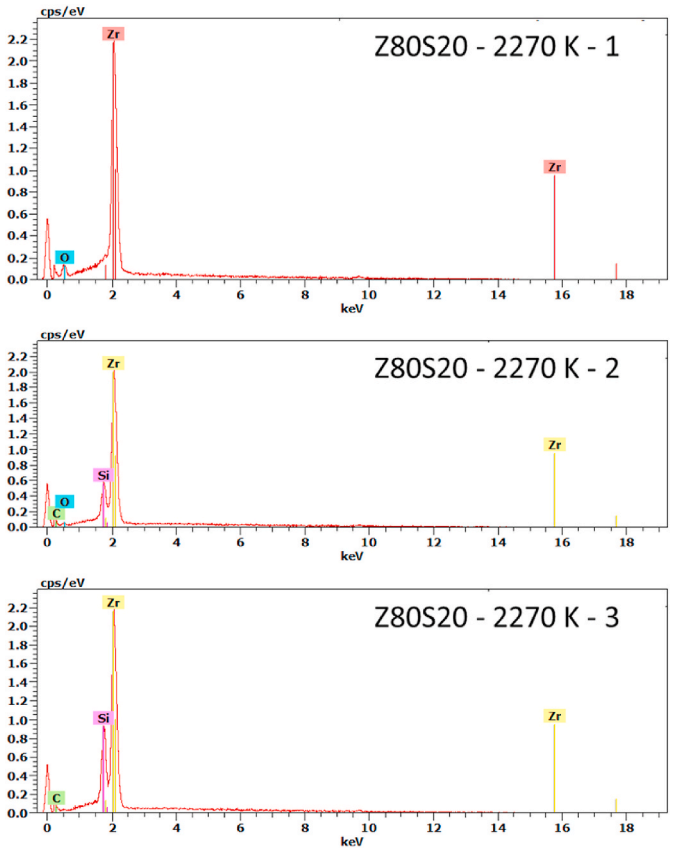

Fig. 15. EDS spectra obtained on the cross-section of the Z80S20 sample oxidized at 2270 K (analysis zones 1, 2 and 3 marked in Fig. 12).

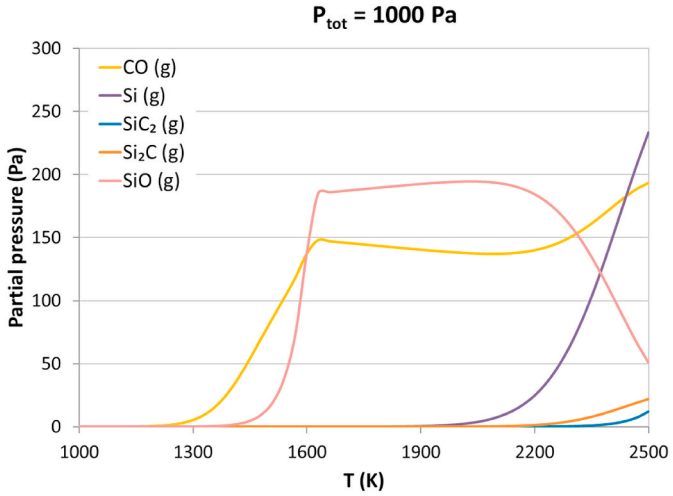

Fig. 16. Thermodynamic calculations for the oxidation of SiC by atomic oxygen at 1000 Pa total air pressure.

3.2. Oxidation in air plasma

During the experiments with the MESOX set-up, the temperature is measured with a monochromatic pyrometer (5 μm) and the solar flux is also recorded. The typical temperature profile of an experiment is presented in Fig. 4, where the temperature is colored in blue and the simultaneous incident solar flux is colored in red. The temperature rise lasts only a few 10 s to reach the plateau at the targeted temperature for 300 s, here around 2600 K. At the end of this plateau, the temperature decreases very quickly due to the rapid closing the shutter.

The oxidation study was performed on several samples for all the composites: H80S20, H70S30, Z80S20 and Z70S30. Fig. 5 provides the photos of the samples after oxidation in air plasma conditions at 1000 Pa depending on the oxidation temperature.

The mass variation by surface area and time was measured between the beginning and the end of the oxidation test and has been reported in Fig. 6 in the temperature range 1750–2650 K, each dot representing one sample.

After oxidation, XRD analyses were conducted on all the oxidized samples to identify the oxide species formed depending on the temperature. Fig. 7 shows the XRD diffractograms for H80S20 from 1770 K to 2400 K where monoclinic hafnia is the main oxide and at 1770 K hafnium diboride is also visible due to the low thickness of the oxide layer. Similar results are obtained for H70S30.

Fig. 8 shows the XRD diffractograms for Z80S20 from 1800 K to 2630 K. Monoclinic zirconia is the main oxide and at 1800 K zirconium diboride is visible for the same reason as for H80S20. A peak at 26.7°, attributed to the most intense peak of $ZrSiO_4$ (ICDD 081–0589) phase is also visible for the lowest temperatures, 1800 K and 1940 K, due to the presence of a glassy phase as confirmed by the SEM images. Others peaks of this phase are present but are overlapped with those of m-ZrO_2. For the highest temperature, cubic zirconia has been identified in low quantity. The XRD patterns for Z70S30 are not presented because similar results were obtained including the presence of zircon at the two lowest temperatures (at 1780 and 1940 K) and of cubic zirconia at 2620 K.

Four oxidation mechanisms have been identified in the mass loss variation with temperature as reported in Fig. 6 and are schematized in Fig. 9 with:

- segment A: a slight mass gain for the lower temperatures (from 1750 to 1950 K),
- segment B: a first notable mass loss,
- segment C: a plateau with a constant mass loss showing an interesting behavior between 2050 and 2250 K, not yet found in the literature,
- segment D: a second significant mass loss.

The different mechanisms or reactions occurring into these four segments are detailed hereafter.

3.2.1. Segment A - 1750 to 1950 K

On segment A, from 1750 to 1950 K, a slight mass gain is observed for each composite, slightly larger for the two ZrB_2-based materials. The mass gain is attributed to both the formation of a borosilicate glass on the surface and the formation of some isolated groups of oxide crystals (ZrO_2 or HfO_2). The SEM images of the surfaces of the samples present some relevant cracks (Fig. 10). They are typical to this type of glassy phase due to the fast cooling at the end of the experiment.

Three equations can describe the phenomena. The first one is the oxidation of the diboride, HfB_2 or ZrB_2, respectively into hafnia or zirconia plus the formation of gaseous B_2O_3 (eq. (3)). At the same time, the oxidation of SiC into silica, and the vaporization of CO occur (eq. (4)). The silica SiO_2 (l, s) interacts with B_2O_3 (g) to form a borosilicate glassy phase on the surface. The formation of the oxide of the diboride that is heavier leads to a mass gain, despite the vaporization of some products (CO and B_2O_3). Karlsdottir et al. have also observed a similar glassy phase (rich in SiO_2) on ZrB_2-15 vol%SiC at 1973 K in rapid oxidation for 15 min [29]. Carney et al. have also seen this glassy phase on the oxidized surface at 1973 K in air, on dense ZrB_2-20 vol%SiC samples sintered by SPS [30].

$$ZrB_2\ (s) + 5\ O\ (g) \rightarrow ZrO_2\ (s) + B_2O_3\ (g) \quad (3)$$

$$SiC\ (s) + 3\ O\ (g) \rightarrow SiO_2\ (l,s) + CO\ (g) \quad (4)$$

$$SiO_2\ (l,s) + B_2O_3\ (g) \rightarrow SiO_2{\cdot}B_2O_3\ (l,s) \quad (5)$$

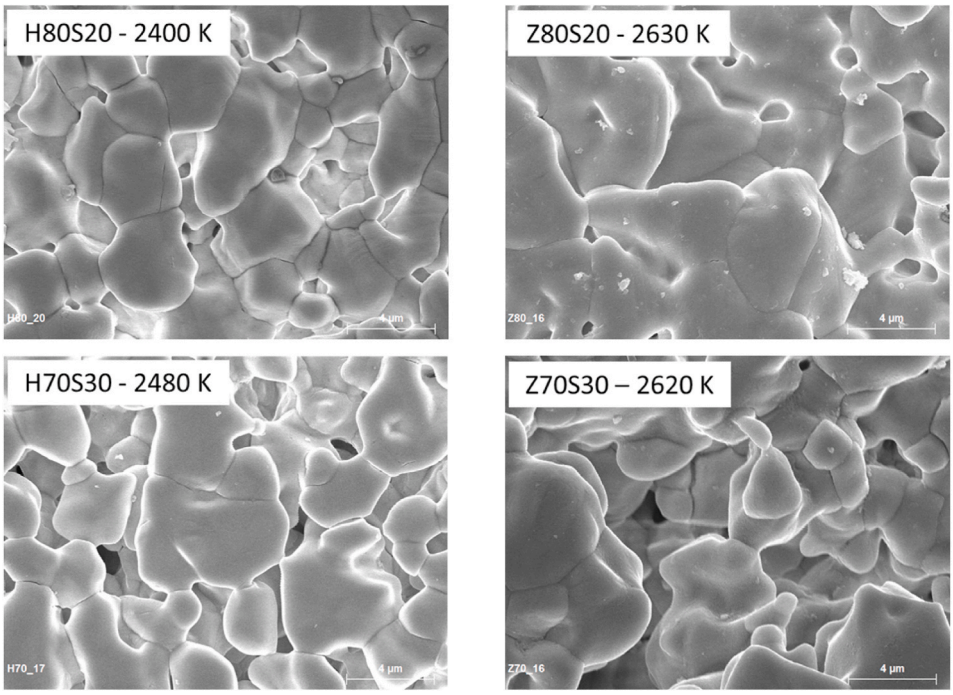

Fig. 17. SEM images of the surfaces of the oxidized samples from segment D (x 6000, scale bar 4 μm).

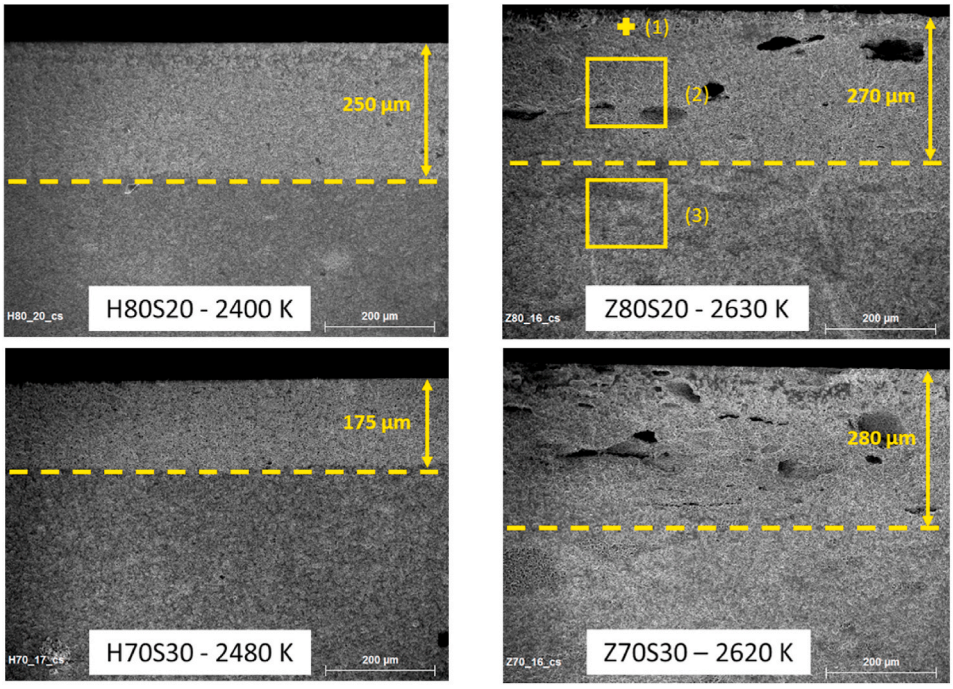

Fig. 18. SEM cross-sections of the oxidized samples at maximal temperatures.

3.2.2. *Segment B – 1950 to 2050 K*

On segment B, a first significant mass loss is measured. A new vaporization phenomenon appears in this temperature range. Vaporization of silica and/or boron oxide began and/or active oxidation of SiC occurs according to Eqs. (6) and (7):

$$SiO_2{\cdot}B_2O_3\ (l,s) \rightarrow SiO\ (g) + O\ (g) + B_2O_3\ (g) \quad (6)$$

$$SiC\ (s) + 2\ O\ (g) \rightarrow SiO\ (g) + CO\ (g) \quad (7)$$

This partial vaporization and/or active oxidation is clearly visible in Fig. 11 with the appearance of some porosities and holes on the surfaces of H70S30 at 2030 K and Z70S30 at 2050 K. On the H70S30 and Z70S30 surfaces, around 2040 K, hafnia (or zirconia) crystals are on the top layer with the glassy phase visible between the grains, previously detailed in Fig. 9, segment B.

At this temperature level, the mass gain induced by the formation or zirconia (or hafnia) is lowered by the simultaneous vaporization of silica and boron oxide and by the active oxidation of SiC that can explain the global mass loss measured (Fig. 6).

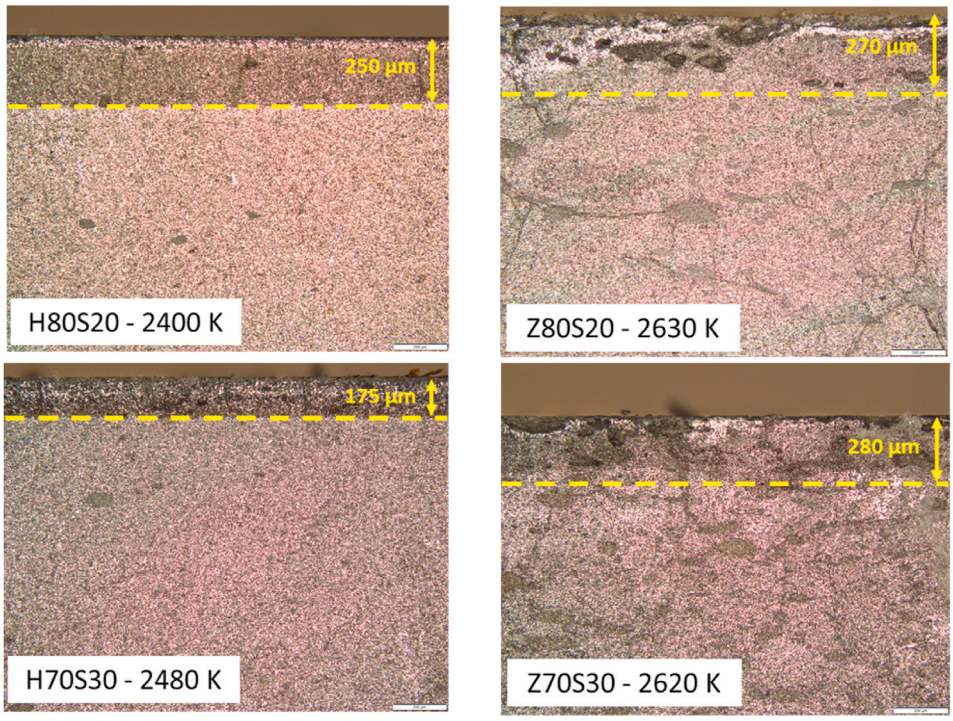

Fig. 19. Optical micrographs of the cross-sections presented in Fig. 18.

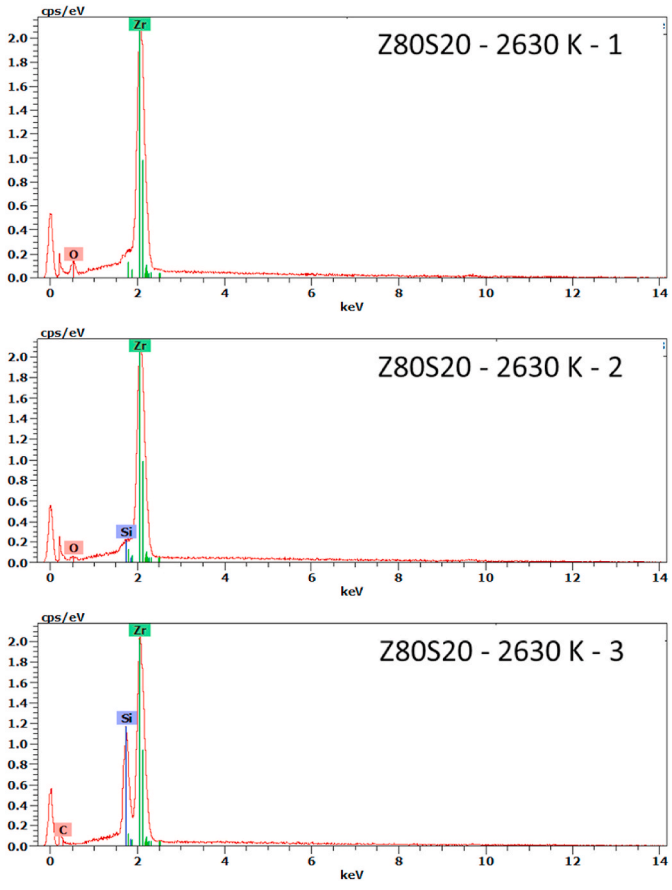

Fig. 20. EDS spectra obtained on the cross-section of the Z80S20 sample (Fig. 16) oxidized at 2600 K.

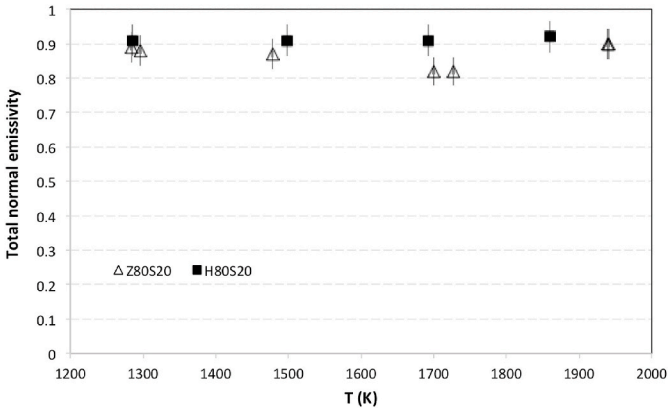

Fig. 21. Total normal emissivity for pre-oxidized samples in air plasma conditions versus temperature measured in air at 1000 Pa.

3.2.3. *Segment C - 2050 to 2250 K*

From 2050 to 2250 K, the mass loss is constant for several samples relative to the initial mass of each sample. A plateau is emerging in this temperature range regardless the SiC amount or the type of diboride (hafnium or zirconium). The mass loss is more significant for samples with 30 vol%SiC (H70S30 and Z70S30) suggesting that the silicon carbide is responsible for this singular behavior. It is important to notice that the Z70S30 composite does not have a clear plateau on the segment C unlike the other composites. A possible explanation would be the association of two phenomena: first, the diffusion rate of oxygen in zirconia that is higher than in hafnia according to Smith et al. [31] and second, the greater amount of SiC leading to more porosity which could accelerate the diffusion of oxygen through the porosities increasing the oxidation of SiC that could result in a faster mass loss.

Fig. 12 presented the SEM images from the surface and cross-section of the Z80S20 oxidized samples from 2040 to 2270 K made to understand and explain the oxidation mechanisms on the plateau of segment C. Similar surface microstructures are observed for all the samples from

the beginning to the end of the plateau: a porous surface with oxide crystals. XRD patterns indicate only one phase, monoclinic HfO_2 or ZrO_2 depending on the type of the initial diboride in this temperature range. A grain growth for ZrO_2 is observed with the increase of temperature from 2040 K to 2270 K. Similar results are obtained for HfB_2-based composites. Fig. 12 also shows the cross-sections of the oxidized samples at three temperatures on the plateau of segment C for Z80S20 and the last one is placed at the limit with segment D (2270 K). The oxidized area is made up of two layers of different compositions. Raman spectra taken at different places of the cross-section for Z80S20 at 2040 K are presented in Fig. 13 to identify the composition of the two visible layers. The top one from 0 (surface) down to 60 μm in depth is composed of m-ZrO_2 (Fig. 13a). m-ZrO_2 phase presents 18 peaks characteristics of Raman active modes of vibration but only 15 have been observed experimentally [32,33]. At 102, 179, 190, 334, 347, 381, 476, 536 and 615 cm^{-1} peaks of the A_g vibration mode are visible. At 223, 306, 501, 558, 572 and 637 cm^{-1} peaks of the B_g vibration mode can be observed. From 70 to 120 μm in depth, no element is visible because ZrB_2 is Raman inactive, this layer is therefore composed of only ZrB_2 and is fully SiC-depleted (Fig. 13b). From 130 to 1000 μm in depth, SiC is visible, characterizing the non-oxidized bulk sample (Fig. 13c) [34]. Two peaks, present in the initial SiC powder, are visible on the Raman spectra. Same results have been obtained for the cross-sections of the other compositions on the plateau of segment C. EDS spectra obtained on the cross-sections of the Z80S20 samples oxidized at 2150 K and 2270 K (Fig. 14 and Fig. 15) confirmed these results. In the first layer, only Zr and O have been identified, a little quantity of Si is detected in the second layer and an important quantity of Si and C is detected in the third layer. From 2040 to 2150 K, the oxide layers composed of ZrO_2 (around 70 μm for 2040 and 2150 K) as well as the SiC-depleted layers have nearly the same thickness (around 40 μm for 2040 and 2150 K). A grain growth appears in the ZrO_2 layer from 2170 K and it is even more noticeable at 2270 K. This can explain that this layer is a bit finer at 2270 K (63 μm) than at 2150 K (72 μm). From 2170 to 2270 K, the thickness of the SiC-depleted layer remains unchanged (around 45 μm).

Hu et al. have tested ZrB_2-30 vol%SiC in a high frequency plasma wind tunnel at 2173 K and they concluded that it had an excellent ablation resistance and stability compared to ZrB_2-10 vol%SiC at 18 000 Pa [20]. This result can be considered quite different from ours as it was shown that a higher amount of SiC resulted in a worst oxidation resistance, characterized by a greater mass loss for Z70S30 and H70S30 than for Z80S20 and H80S20 at 2280 K (the end of the segment C).

Thermodynamic calculations have been carried out with the module equilibrium composition from HSC Chemistry® software (Metso Outotec). The calculation is based on the Gibbs energy minimization and it permits to understand the oxidation mechanisms occurring on the plateau of mass variation. Calculations have been conducted on SiC only to highlight its role in the oxidation mechanisms.

Fig. 16 shows the results of the thermodynamic calculation carried out for the oxidation of SiC by atomic oxygen at 1000 Pa total air pressure, corresponding to the experimental conditions, and the predominant reaction is Eq. (7), with the formation of SiO (g) and CO (g) from 1600 up to 2250 K (Plateau on segment C). Above this temperature (Segment D), the global reaction of Eq. (8) is predominant and consumes more SiC that can lead to a greater mass loss due to the formation of gaseous species, the main one being Si (g) followed in lower proportion by Si_2C (g) and SiC_2 (g):

$$4\ SiC\ (s) + O\ (g) \rightarrow Si\ (g) + SiC_2\ (g) + Si_2C\ (g) + CO\ (g) \quad (8)$$

The experimental temperatures corresponding to the formation of SiO and CO and on the other side of Si, Si_2C and SiC_2 are a little bit different from the ones obtained by the thermodynamic calculation due to non-equilibrium conditions but the trend is the same.

3.2.4. Segment D – 2250 K to T_{max}

The maximal temperature reached during the oxidation is lower for HfB_2-based materials than for the ZrB_2 ones. The solar experiments did not allow reaching higher temperatures than 2400 K (H80S20) or 2480 K (H70S30) for the HfB_2-composites this being due possibly to the fact that hafnia formed by oxidation less absorbs the concentrated solar radiation.

At the maximal temperature for each composition, similar microstructures are observed for all the samples: a porous surface with big oxide crystals (Fig. 17). Oxide grains are larger than those observed for the samples of the plateau of segment C due to the higher temperature. XRD patterns indicate only one phase, for HfB_2-based composites, which is monoclinic HfO_2. For ZrB_2-based composites, cubic zirconia appears as a secondary phase in addition to monoclinic zirconia. Indeed, oxygen vacancies can stabilize c-ZrO_2 in small quantities [35–37].

Fig. 18 shows the cross sections of the different composites at the maximal temperature reached in this study. The oxidized layer is composed only of zirconia or hafnia according to EDS analysis shown in Fig. 20 (for Z80S20 sample oxidized at 2630 K). Optical micrographs show only one oxide layer for all the compositions (Fig. 19). At this temperature level, the SiC-depleted layer no longer exists possibly due to the important thickness of the oxide layer. An assumption is that the rapid vaporization of SiC, according to reaction 8 (Fig. 14), promotes only the formation of a huge oxide layer composed only of zirconia or hafnia and thus the oxygen could no longer diffuse deeply into the material. At the highest temperature level, H70S30 presents a finer oxide layer (175 μm) than H80S20 (250 μm). It is confirmed by the mass loss of H70S30 being lower than for H80S20. HfB_2-based composites have a dense oxide layer. H70S30 seems to have a better oxidation behavior than H80S20. According to Sevastyanov et al. under dissociated oxygen, around 2873 K, HfB_2-20 vol%SiC has a better behavior for porous samples (35% porosity) than samples with 10 or 15 vol% SiC sintered by SPS [22]. In this study, the monolithic HfB_2-30 vol%SiC seems to be the most resistant for oxidation up to 2470 K.

ZrB_2-based composites have an oxide layer with holes possibly due to the rapid vaporization of SiC that is not compensated by the growth of zirconia grains. Z70S30 presents the thickest oxide layer (280 μm) according to the highest mass loss compared to the Z80S20 composite with the lowest mass loss. Z80S20 seems to present the better oxidation resistance even if the thickness of oxide layer is around 270 μm i.e., 10% of the original sintered body. Finally, it seems that SiC is not the most suitable additional compound for this range of temperature because it does not enough protect from oxidation at such high temperature.

To conclude, these composites can be classified in the following order for their oxidation resistance: in first position, Z80S20 with the lowest mass loss at 2630 K, then H70S30 with a lower mass loss than H80S20 and a thinner oxide layer, in third position, H80S20 with an oxide layer of 250 μm and finally, Z70S30 which has the higher mass loss at 2620 K, the thickest oxide layer with a lot of holes.

3.3. Total normal emissivity

Total emissivity is an important parameter for heat flux calculation during a hypersonic reentry of a space vehicle. To reject more heat and avoid the thermal degradation of the material, the emissivity needs to be the highest (closer to 1).

Before the emissivity measurements, the Z80S20 and H80S20 samples have been pre-oxidized in the MESOX facility in air plasma at 2280 K and 2220 K respectively to obtain a similar surface in terms of microstructure and chemical composition than those obtained in the oxidation study. Data obtained for the total normal emissivity versus temperature at 1000 Pa total air pressure for the two different samples Z80S20 and H80S20 are presented in Fig. 21. The total normal emissivity is quite constant in the temperature range for the two compositions considering the uncertainty (5%), the emissivity is around 0.9 for HfB_2-based composite, and 0.88 for ZrB_2-based material.

Radiative properties of ZrB_2–SiC composites have been measured by Scatteia et al. [38] and Meng et al. [39] with two different methods and different surface state and/or compositions. Scatteia et al. have measured directly the total directional radiance of ZrB_2-20 vol%SiC oxidized in situ at 200 Pa total pressure with the MEDIASE set-up using a radiometer [38]. Meng et al. have used FTIR spectrometer to measure the spectral emissivity on several ZrB_2-20 vol%SiC-15 vol%C samples pre-oxidized in an induction furnace in the 1373–2073 K temperature range at atmospheric pressure [39]. The total hemispherical emissivity measured at 1680 K by Scatteia et al. gives a value of 0.72, much lower than the one we have obtained (0.83 at 1700 K), because the oxidation was done in situ in contrast with our protocol where the samples were pre-oxidized in air plasma before emissivity evaluation. Meng et al. have measured 0.78 at 1873 K that is different from our result of 0.90 at 1940 K, due to the difference in the initial composition (presence of carbon).

4. Conclusion

The oxidation of fully-dense diboride samples containing two amounts of SiC was studied in atmospheric re-entry conditions, at low total air pressure of 1000 Pa and from 1750 up to 2600 K ZrB_2-based composites presents a better oxidation resistance at high temperature, especially the one with 20 vol% SiC which has the lowest mass loss after 300 s at 2600 K under dissociated air with atomic oxygen. An oxidation mechanism of these composites was proposed and it is decomposed into four parts:

- from 1750 to 1950 K, the passive oxidation of SiC occurs with the formation of a borosilicate glassy phase and a slight mass gain, together with the formation of some zirconia or hafnia isolated crystals,
- from 1950 to 2050 K, a first mass loss, greater for composites containing 30 vol% SiC, occurs due to two coexisting phenomena: the partial vaporization of the borosilicate phase and the formation of zirconia or hafnia,
- from 2050 to 2250 K, a plateau of constant mass loss, due to the active oxidation of SiC into SiO (g) and CO (g) with the formation of zirconia or hafnia crystalline layer is observed, which had never been shown before in the literature,
- from 2250 K up to 2600 K, a second significant mass loss due to the active oxidation of SiC into Si (g), SiC_2 (g) and Si_2C (g) together with the formation of a zirconia or hafnia layer is measured.

According to these results, SiC is not the most suitable additional compound for aerospace applications to protect against oxidation in air plasma conditions at very high temperature due to the significant mass loss from 2300 K. Other additions such as $TaSi_2$ and AlN are under study to protect more efficiently against oxidation.

Declaration of competing interest

The authors declare that they have no known competing financial interests or personal relationships that could have appeared to influence the work reported in this paper.

Acknowledgments

The authors want to thank J.-L. Sans from PROMES-CNRS for the emissivity measurements and M. Vandenhende from IRCER lab for the technical support during the sintering of the samples.

This work was partially funded by the Région Occitanie, France under the contract number 2018001076 ALDOCT-000472, CNRS n° 173239 and FEDER-FSE under the contract number 2018-001076-01, CNRS n°179222 through the PhD funding of C. Pellegrini.

References

[1] M.M. Opeka, I.G. Talmy, J.A. Zaykoski, Oxidation-based materials selection for 2000°C + hypersonic aerosurfaces: theoretical considerations and historical experience, J. Mater. Sci. 39 (2004) 5887–5904.
[2] W.G. Fahrenholtz, G.E. Hilmas, Ultra-high temperature ceramics: materials for extreme environments, Scripta Mater. 129 (2017) 94–99, https://doi.org/10.1016/j.scriptamat.2016.10.018.
[3] W.G. Fahrenholtz, G.E. Hilmas, I.G. Talmy, J.A. Zaykoski, Refractory diborides of zirconium and hafnium, J. Am. Ceram. Soc. 90 (2007) 1347–1364, https://doi.org/10.1111/j.1551-2916.2007.01583.x.
[4] E.V. Clougherty, D. Kalisch, E.T. Peters, Research and Development of Refractory Oxidation-Resistant Diborides, Tech. Rept. AFML-TR-68-190, July 1968.
[5] W.C. Tripp, H.H. Davis, H.C. Graham, Effetc of an SiC addition on the oxidation of ZrB_2, Ceram. Bull. 52 (8) (1973) 612–616.
[6] P.A. Williams, R. Sakidja, J.H. Perepezko, P. Ritt, Oxidation of ZrB_2–SiC ultra-high temperature composites over a wide range of SiC content, J. Eur. Ceram. Soc. 32 (2012) 3875–3883, https://doi.org/10.1016/j.jeurceramsoc.2012.05.021.
[7] R. Inoue, Y. Arai, Y. Kubota, Oxidation behaviors of ZrB_2–SiC binary composites above 2000°C, Ceram. Int. 43 (2017) 8081–8088, https://doi.org/10.1016/j.ceramint.2017.03.129.
[8] W.B. Han, P. Hu, X.H. Zhang, J.C. Han, S.H. Meng, High-temperature oxidation at 1900°C of ZrB_2-xSiC ultra high temperature ceramic composites, J. Am. Ceram. Soc. 91 (10) (2008) 3328–3334, https://doi.org/10.1111/j.1551-2916.2008.02660.x.
[9] C.M. Carney, Oxidation resistance of hafnium diboride-silicon carbide from 1400 to 2000 °C, J. Mater. Sci. 44 (2009) 5673–5681, https://doi.org/10.1007/s10853-009-3799-7.
[10] C. Piriou, O. Rapaud, S. Foucaud, L. Charpentier, M. Balat-Pichelin, M. Colas, Sintering and oxidation behavior of HfB_2-SiC composites from 0 to 30 vol% SiC between 1450 and 1800 K, Ceram. Int. 45 (2019) 1846–1856, https://doi.org/10.1016/j.ceramint.2018.10.075.
[11] N. Li, P. Hu, X. Zhang, Y. Liu, W. Han, Effects of oxygen partial pressure and atomic oxygen on the microstructure of oxide scale of ZrB_2–SiC composites at 1500 °C, Corrosion Sci. 73 (2013) 44–53, https://doi.org/10.1016/j.corsci.2013.03.023.
[12] Y.H. Seong, D.K. Kim, Oxidation behavior of ZrB_2-xSiC composites at 1500°C under different oxygen partial pressures, Ceram. Int. 40 (2014) 15303–15311, https://doi.org/10.1016/j.ceramint.2014.07.036.
[13] C. Tian, D. Gao, Y. Zhang, C. Xu, Y. Song, X. Shi, Oxidation behaviour of zirconium diboride-silicon carbide ceramic composites under low oxygen partial pressure, Corrosion Sci. 53 (2011) 3742–3746, https://doi.org/10.1016/j.corsci.2011.07.020.
[14] Y. Yang, M. Li, L. Xu, J. Xu, Y. Qian, J. Zuo, T. Li, Oxidation behaviours of ZrB_2-SiC-$MoSi_2$ composites at 1800 °C in air with different pressures, Corrosion Sci. 157 (2019) 87–97, https://doi.org/10.1016/j.corsci.2019.05.027.
[15] B. Du, N. Li, B. Ke, P. Xing, X. Jin, P. Hu, X. Zhang, ZrB_2-SiC composites' surface temperature response to dissociated oxygen at 1600°C, Ceram. Int. 42 (2016) 14292–14297, https://doi.org/10.1016/j.ceramint.2016.06.041.
[16] S. Mungiguerra, A. Cecere, R. Savino, F. Saraga, F. Monteverde, D. Sciti, Improved aero-thermal resistance capabilities of ZrB_2-based ceramics in hypersonic environment for increasing SiC content, Corrosion Sci. 178 (2021) 109067, https://doi.org/10.1016/j.corsci.2020.109067.
[17] M. Gasch, S. Johnson, Physical characterization and arcjet oxidation of hafnium-based ultra high temperature ceramics fabricated by hot pressing ans field-assisted sintering, J. Eur. Ceram. Soc. 30 (2010) 2337–2344. https://doi:10.1016/j.jeurceramsoc.2010.04.019.
[18] D.L. Poerschke, M.D. Novak, N. Abdul-Jabbar, S. Krämer, C.G. Levi, Selective active oxidation in hafnium boride-silicon carbide composites above 2000°C, J. Eur. Ceram. Soc. 36 (2016) 3697–3707, https://doi.org/10.1016/j.jeurceramsoc.2016.05.048.
[19] J. Marschall, D.A. Pejakovic, W.G. Farenholtz, G.E. Hilmas, S. Zhu, J. Ridge, D. G. Fletcher, C.O. Asma, J. Thömel, Oxidtaion of ZrB_2-SiC ultrahigh-temperature ceramic composite in dissociated air, J. Thermophys. Heat Tran. 23 (2) (2009) 267–278, https://doi.org/10.2514/1.39970.
[20] P. Hu, K. Gui, Y. Yang, S. Dong, X. Zhang, Effect of SiC content on the ablation and oxidation behavior of ZrB_2-based ultra high temperature ceramic composites, Materials 6 (2013) 1730–1744, https://doi.org/10.3390/ma6051730.
[21] V.G. Sevastyanov, E.P. Simonenko, A.N. Gordeev, N.P. Simonenko, A. F. Kolesnikov, E.K. Papynov, O.O. Shichalin, V.A. Avramenko, N.T. Kuznetsov, HfB_2-SiC (45 vol %) ceramic material: manufacture and behavior under long-term exposure to dissociated air jet flow, Russ. J. Inorg. Chem. 59 (11) (2014) 1298–1311, https://doi.org/10.1134/S0036023614110217.
[22] V.G. Sevastyanov, E.P. Simonenko, A.N. Gordeev, N.P. Simonenko, A. F. Kolesnikov, E.K. Papynov, O.O. Shichalin, V.A. Avramenko, N.T. Kuznetsov, HfB_2-SiC (10-20 vol %) ceramic materials: manufacture and behavior under long-term exposure to dissociated air streams, Russ. J. Inorg. Chem. 59 (12) (2014) 1361–1382, https://doi.org/10.1134/S0036023614120250.
[23] V.G. Sevastyanov, E.P. Simonenko, A.N. Gordeev, N.P. Simonenko, A. F. Kolesnikov, E.K. Papynov, O.O. Shichalin, V.A. Avramenko, N.T. Kuznetsov, Behavior of a sample of the ceramic material HfB_2-SiC (45 vol%) in the flow of dissociated air and the analysis of the emission spectrum of the boundary layer above its surface, Russ. J. Inorg. Chem. 60 (11) (2015) 1360–1373, https://doi.org/10.1134/S0036023615110133.
[24] J. Han, P. Hu, X. Zhang, S. Meng, W. Han, Oxidation-resistant ZrB_2–SiC composites at 2200 °C, Compos. Sci. Technol. 68 (2008) 799–806, https://doi.org/10.1016/j.compscitech.2007.08.017.

[25] C.M. Carney, A. Paul, S. Venugopal, T. Parthasarathy, J. Binner, A. Katz, P. Brown, Qualitative analysis of hafnium diboride based ultra high temperature ceramics under oxyacetylene torch testing at temperatures above 2100°C, J. Eur. Ceram. Soc. 34 (2014) 1045–1051, https://doi.org/10.1016/j.jeurceramsoc.2013.11.018.
[26] M.J.H. Balat, Determination of the active-to-passive transition in the oxidation of silicon carbide in standard and microwave-excited air, J. Eur. Ceram. Soc. 16 (1996) 55–62, https://doi.org/10.1016/0955-2219(95)00104-2.
[27] M. Balat-Pichelin, A. Vesel, Neutral oxygen atom density in the MESOX air plasma solar furnace facility, Chem. Phys. 327 (2006) 112–118, https://doi.org/10.1016/j.chemphys.2006.03.034.
[28] M. Balat-Pichelin, J.L. Sans, E. Bêche, L. Charpentier, A. Ferrière, S. Chomette, Emissivity at high temperature of Ni-based superalloys for the design of solar receivers for future tower power plants, Sol. Energy Mater. Sol. Cells 227 (2021) 111066, https://doi.org/10.1016/j.solmat.2021.111066.
[29] S.N. Karlsdottir, J.W. Halloran, Rapid oxidation characterization of ultra-high temperature ceramics, J. Am. Ceram. Soc. 90 (2007) 3233–3238, https://doi.org/10.1111/j.1551-2916.2007.01861.x.
[30] C.M. Carney, P. Mogilvesky, T.A. Parthasarathy, Oxidation behavior of zirconium biboride silicon carbide produced by the Spark Plasma Sintering method, J. Am. Ceram. Soc. 92 (2009) 2046–2052, https://doi.org/10.1111/j.1551-2916.2009.03134.x.
[31] A.W. Smith, F.W. Meszaros, C.D. Amata, Permeability of zirconia, hafnia, and thoria to oxygen, J. Am. Ceram. Soc. 49 (1966) 240–244, https://doi.org/10.1111/j.1151-2916.1966.tb13248.x.
[32] S.N. Tkachev, M.H. Manghnani, A. Niilisk, J. Aarik, H. Mändar, Micro-Raman spectroscopy and X-ray diffraction studies of atomic-layer-deposited ZrO_2 and HfO_2 thin films, J. Mater. Sci. 40 (2005) 4293–4298, https://doi.org/10.1007/s10853-005-2826-6.
[33] D.A. Daramola, M. Muthuvel, G.G. Botte, Density functional theory analysis of Raman frequency modes of monoclinic zirconium oxide using Gaussian basis sets and isotopic substitution, J. Phys. Chem. B 114 (2010) 9323–9329, https://doi.org/10.1021/jp9077135.
[34] S. Nakashima, K. Tahara, Raman scattering determination of structures for SiC polytypes: quantitative evaluation with a revised model of lattice dynamics, Phys. Rev. B 40 (1989) 6339–6344, https://doi.org/10.1103/PhysRevB.40.6339.
[35] E.V. Stefanovich, A.L. Shluger, C.R.A. Catlow, Theoretical study of the stabilization of cubic-phase ZrO_2 by impurities, Phys. Rev. B 49 (17) (1994) 11560–11573.
[36] S. Fabris, A.T. Paxton, M.W. Finnis, A stabilization mechanism of zirconia based on oxygen vacancies only, Acta Mater. 50 (2002) 5171–5178.
[37] P. Kalita, S. Saini, P. Rajput, S.N. Jha, D. Bhattacharyya, S. Ojha, D.K. Avasthi, S. Bhattacharya, S. Ghosh, Oxygen vacancy mediated cubic phase stabilization at room temperature in pure nano-crystalline zirconia films: a combined experimental and first-principles based investigation, Phys. Chem. Chem. Phys. 21 (2019) 22482–22490, https://doi.org/10.1039/C9CP02121C.
[38] L. Scatteia, R. Borrelli, G. Cosentino, E. Beche, J.L. Sans, M. Balat-Pichelin, Catalytic and radiative behaviors of ZrB_2-SiC ultrahigh temperature ceramic composites, J. Spacecraft Rockets 43 (2006) 1004–1012, https://doi.org/10.2514/1.21156.
[39] S. Meng, H. Chen, J. Hu, Z. Wang, Radiative properties characterization of ZrB_2-SiC-based ultrahigh temperature ceramic at high temperature, Mater. Des. 32 (2011) 377–381, https://doi.org/10.1016/j.matdes.2010.06.007.